



Study of Mechanical, Electronic and Optical Characteristics for AuBiF₃ Material

Nassah Younes^{1,*}, Benmakhlouf Abdenour², Remache El Ouardi³

¹ department of ST University of Ammar Thelidji Laghouat, Algeria, y.nassah@lagh-univ.dz

² department of ST University of Ammar Thelidji Laghouat, Algeria, a.benmakhlouf@lagh-univ.dz

³ University of Laarbi Ben M'hidi Oum El Bouaghi, Algeria, rlouardi@yahoo.fr

*Corresponding author:(Nassah Younes), Email: y.nassah@lagh-univ.dz

Abstract

In this study, we present an ab initio theoretical study of the mechanical, electronic, and optical properties of AuBiF₃ using ultrasoft pseudopotentials within the framework of density functional theory (DFT). Our investigation shows the formation energy is negative, which indicates that the material is stable thermodynamically. The elastic properties show that the studied perovskite satisfies the Born stability criteria, confirming its mechanical stability. Additionally, the Pugh ratio (B/G) exceeds 1.75, indicating that the material exhibits ductility. The electronic band gap indicates that this material is a semiconductor with a direct M-M band gap of 1.51 eV, as determined using the HSE06 functional, making it suitable for solar energy applications. An examination of the optical properties shows that the absorption coefficient exhibits significant absorption in the visible range, on the order of 10⁴ cm⁻¹, along with strong ultraviolet absorption, also on the order of 10⁴ cm⁻¹. Our findings suggest that the investigated material possesses notable characteristics, making it promising for solar cell applications and other optoelectronic devices.

Keywords: Perovskite; Absorption; Ductile; Solar Cells; Semiconductor.

<https://doi.org/10.63070/jesc.2025.045>

Received 10 July 2025; Revised 16 November 2025; Accepted 17 December 2025;

Available online 24 December 2025.

Published by Islamic University of Madinah on behalf of *Islamic University Journal of Applied Sciences*.

This is a free open access article under the Creative Attribution (CC.BY.4.0) license.

1. Introduction

The global energy landscape is facing major challenges resulting from a combination of critical factors, including climate change, the constant increase in energy demand linked to population growth, large-scale industrialization, and the progressive scarcity of conventional fossil fuels [1]. The climate emergency and economic constraints are driving scientific and industrial communities to develop renewable and sustainable energy solutions [2]. Solar energy is the most promising alternative among the existing sources due to its nearly infinite supply and demand, compatibility with large-scale activities, and low environmental impact [3]. This dynamic has resulted in deep study into new functional materials that can improve the performance of optoelectronic devices, particularly photovoltaic cells (PVCs) [4]. The target materials must have desirable optical properties such as a high absorption coefficient, high optical conductivity, low reflection, and compatibility with low-cost manufacturing techniques [5]. Halogenated perovskites (PHs) with the formula ABX_3 , where A and B are organic or inorganic cations and X is a halogen anion, have received lot of attention [6]. These materials have proven to be particularly versatile, with applications ranging from solar cells [7] to light-emitting diodes (LEDs) [8], advanced optoelectronic devices [9], and lasers [10]. Perovskite solar cells are notable in the photovoltaic sector for their exceptional electrical and optical properties: extended carrier lifetime, high electron mobility, low exciton binding energy, high absorption capacity in the visible spectrum, and intrinsic tolerance to crystal defects [11].

These advantages position PSCs as highly promising materials for PV applications, where the efficiency of PSCs has seen a dramatic improvement, with the PCE increasing from 3.8 % in 2009 [12] to an impressive 28 % these years [13]. This development is the result of multiple strategies, such as bandgap engineering, interface modification, chemical composition optimization, and defect encapsulation and passivation to limit non-radiative losses [14]. Current theoretical models estimate that the theoretical maximum efficiency of these cells could reach approximately 31.1% [15]. These advances confirm the disruptive potential of halogenated perovskites in next-generation solar technologies and justify the continued exploration of new compositions, device architectures and structural modifications to reconcile high performance and long-term stability.

To advance research in this field, we propose the exploration of new compounds from the halogenated perovskite family, which remain largely unexplored both theoretically and experimentally. To this end, we selected the compound $AuBiF_3$ for an in-depth study based on density functional theory (DFT). The results obtained reveal that this material exhibits a direct bandgap of around 1.51 eV, a crucial characteristic for multijunction solar cells to optimize solar spectral capture and maximize conversion efficiency [16, 17]. This study will provide important information on electronic, elastic, and optical

properties in order to better understand its potential in solar cell applications. Our work seeks to give a complete characterization of the fundamental properties of AuBiF_3 , allowing us to assess its potential for next-generation solar technology. These findings will help to expand the database of functional materials suited to solar energy and may open up new pathways in the construction of high-efficiency solar cells, particularly in multi-layer topologies where band gap optimization is a critical factor.

2. Calculation detail

All calculations presented in this study were performed using the pseudopotential and plane-wave method, as implemented in the ab initio simulation code CASTEP [18]. The treatment of the electron exchange-correlation energy was performed using the generalized gradient approximation (GGA) with the Perdew–Burke–Ernzerhof (PBE) parameterization [19]. For better accuracy in band gap estimation, complementary electronic structure calculations were performed using the hybrid Heyd–Scuseria–Ernzerhof (HSE06) functional [20]. The interactions between ionic cores and valence electrons were described using pseudopotentials method [21]. Kohn-Sham wave functions were developed on a plane-wave basis with a cutoff energy set at 600 eV [22]. The Brillouin zones were discretized according to the Monkhorst-Pack scheme [23] with a $6 \times 6 \times 6$ mesh for structural relaxations and $12 \times 12 \times 12$ for electronic and optical calculations. The mechanical properties of the polycrystalline phases were then evaluated from the constants C_{ij} using the Voigt-Reuss-Hill scheme [24].

3. Structural characteristics

AuBiF_3 compounds crystallize in a cubic perovskite-like structure ABX_3 , belonging to the space group $\text{Pm}\bar{3}\text{m}$ with a number of formulas per unit cell $Z = 1$. In this configuration, Bi^{3+} ions occupy B sites and are octahedral coordinated by six fluorine (F^-) ions, while Au^+ ions reside in A sites, at the center of a cub octahedral cage formed by twelve fluorine ions. The unit cell of the AuBiF_3 perovskite lattice is represented in Figure 1. Before undertaking electronic structure calculations using density functional theory (DFT), a first assessment of the geometric stability of the perovskite phase was performed by applying the semi-empirical Goldschmidt model [28]. This model predicts the crystallographic feasibility of structure based on the tolerance factor, defined by the following equation:

$$t = (r_A + r_x)/\sqrt{2}(r_B + r_x) \quad (1)$$

The variables represent the site X, respectively. The Goldschmidt tolerance factor (t) is a useful parameter for estimating the stable structure of the studied material. When t is close to 1, it indicates an ideal cubic structure, while values between 0.8 and 1.0 suggest the potential stability of a distorted

perovskite phase. The calculated tolerance factor of the investigated compounds exhibits 0.916, which suggests higher stability in the cubic structure. Table 1 summarizes the obtained results

Table 1. ionic radii R_i , tolerance factor t , calculated total energy E_{Tot} , AuBiF₃ perovskite.

Material		R_i	a	t	E_{Tot}	H_f
AuBiF ₃	Au	1.37	4.57	0.81	-3051	-1.74
	Bi	1.07				
	F	1.33				

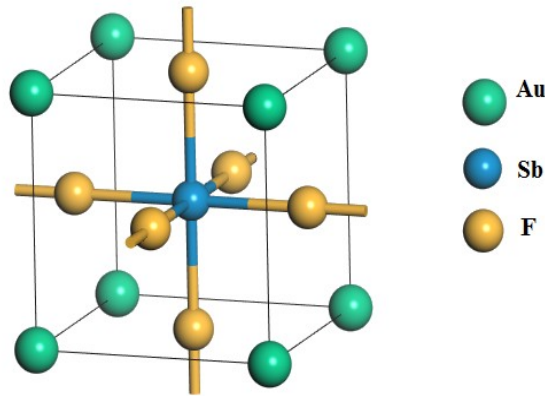


Figure 1. The cubic perovskite structures of AuBiF₃. The Au, Bi and F atoms are all in special Wyckoff positions: 1a: (0,0,0), 1b: (1/2,1/2,1/2) and 3c: (1/2,1/2,0), respectively.

4. Elastic properties

The stiffness and strength of crystalline materials can be assessed via their single-crystal elastic constants. Table 2 presents the values of C_{11} , C_{12} , and C_{44} for the examined compound, ascertained by the strain-stress method [25], elucidating its dynamic response and deformation characteristics under an applied load. The elastic constants were utilized to calculate additional mechanical parameters, including bulk modulus (B), Pugh's ratio (B/G), Young's modulus (E).

The examined material met the Born stability criteria [26] :

$$C_{11} - C_{12} > 0, C_{12} > 0, C_{11} > 0, C_{11} + 2C_{12} > 0, \text{ and } C_{12} < B < C_{11}$$

The bulk modulus (B) quantifies a material's resistance to uniform compression and signifies the extent of resistance during volumetric deformation. Table 2 indicates that the material possesses a high bulk modulus, signifying substantial resistance to hydrostatic pressure.

Young's modulus quantifies the stiffness of an elastic material, defined as the ratio of stress to

strain. The moderate Young's modulus (E) further elucidates the compound's softness. Table 2 illustrates that the current compound has a moderate value, signifying that it deforms more readily under applied stresses and undergoes greater elastic strain compared to stiffer materials with elevated Young's moduli.

The B/G ratio represents the brittleness or ductility of solids [27]. The number above 1.75 implies ductile material, whereas lower values suggest brittle material. The B/G ratio reaches 11.75, demonstrating the ductile nature and flexibility without fracture of the investigated perovskite, which displays high plasticity, which is useful for electronic materials. The obtained results are revealed in the table 2.

TABLE 2. Elastic constants C_{ij} , bulk modulus $B(GPa)$, shear modulus $G(GPa)$, B/G ratio, and Young's modulus $E(GPa)$ of $AuBiF_3$.

Material	C_{11}	C_{12}	C_{44}	B	B/G	E
$AuBiF_3$	138	23	0.25	61	11.75	33

5. Electronic properties

Electronic band structure is a fundamental tool for characterizing the energy states accessible to electrons in a crystal. From the relaxed geometric configurations, we calculated the band structure of the halogenated perovskite compound $AuBiF_3$ using density functional theory (DFT) within the generalized gradient approximation (GGA) framework, according to the Perdew–Burke–Ernzerhof (PBE) parameterization, as implemented in the CASTEP code. The electronic band dispersion was determined along the high-symmetry directions of the first Brillouin zone. The results are presented in Figure 2, for an energy window extending from -15 to 15 eV. The analysis reveals that the valence band maximum (VBM) and the conduction band minimum (CBM) are located at the M point of the Brillouin zone. This configuration confirms that $AuBiF_3$ is a direct bandgap semiconductor, characterized by an (M_c-M_v) -type electronic transition. To obtain a more precise estimate of the bandgap, additional calculations were performed using the hybrid Heyd–Scuseria–Ernzerhof (HSE06) functional. The findings indicate a direct bandgap value of 1.51 eV. This significant value places $AuBiF_3$ as promising compound used in multijunction photovoltaic architectures for high-efficiency solar energy conversion devices[16, 17].

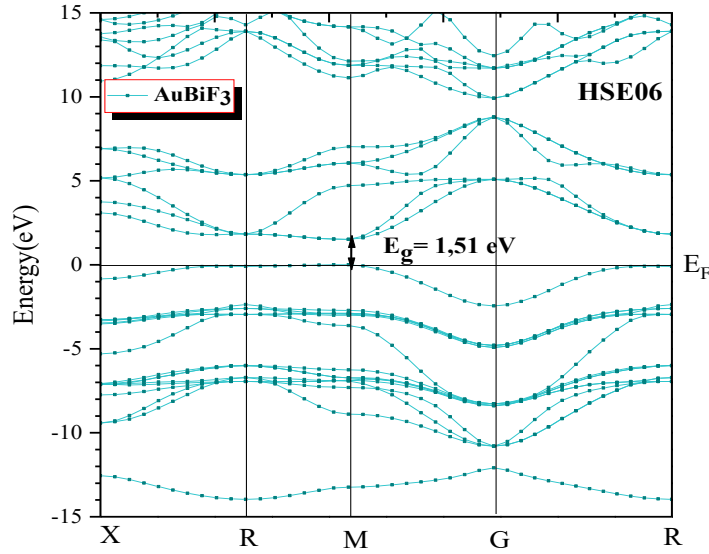


Figure 2. Band structure calculated in high symmetry direction using HSE06 for AuBiF₃ perovskites.

Electronic densities of states (DOS) provide valuable information on the contribution of atomic orbitals to the valence and conduction bands and therefore allow the identification of the electronic origin of the material's band gap. As illustrated in Figure 3, the valence band of both AuBiF₃, located between -12.5 and -5 eV, is dominated by the F-p orbitals with few contribution of Bi: s-p orbitals. Near the Fermi level, the maximum valence band (VBM), which extends from 0 eV to -2.5 eV, is predominantly occupied by Au-d orbitals. The conduction band minimum (CBM) is mainly formed by Bi-p orbitals, while the rest of the conduction band is generated by Au-p and Bi-s orbitals. It can be deduced that the band gap energy of AuBiF₃ is mainly formed by Au-d in (VBM) and Bi-p in (CBM).

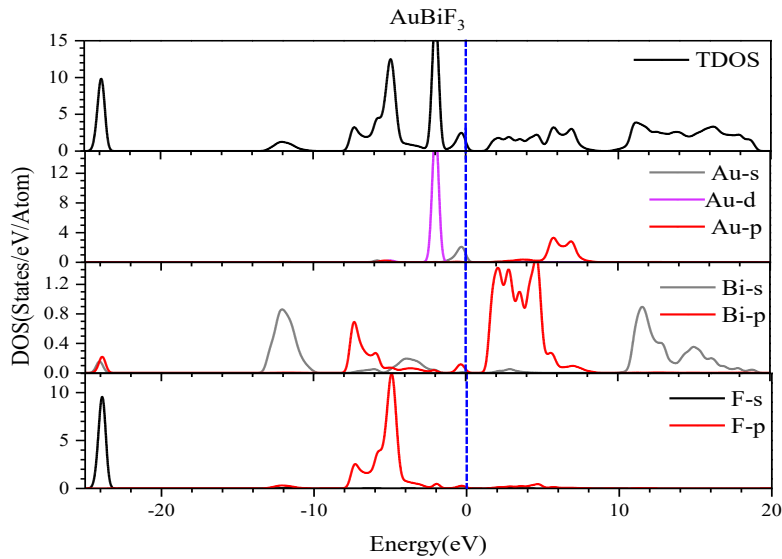


Figure 3. Total (TDOS) and partial density of states (PDOS) calculated using GGA-PBE for AuBiF₃ perovskite.

6. Optical properties

The optical properties of the materials under consideration were investigated throughout a wide spectrum (0 to 25 eV), allowing for an extensive analysis of their electromagnetic response to incident radiation. The complex dielectric function [28], which consists of real $\varepsilon_1(\omega)$ and imaginary $\varepsilon_2(\omega)$ parts, given through the relation

$$\varepsilon(\omega) = \varepsilon_1(\omega) + i\varepsilon_2(\omega)$$

the imaginary part of the dielectric function $\varepsilon_2(\omega)$ can be obtained using the following equation [29] :

$$\varepsilon_2(\omega) = \frac{2\pi e^2}{m_e^2 \omega^2 \varepsilon_0} \sum_{c,v} \int_{BZ} |\langle \psi_k^c | \vec{P}_i | \psi_k^v \rangle|^2 \delta(E_k^c - E_k^v - \hbar\omega) dk^3 \quad (9)$$

the real dielectric function $\varepsilon_1(\omega)$ is derived from $\varepsilon_2(\omega)$ through the Kramers-Kronig [30] relation given by the relation bellow:

$$\varepsilon_1(\omega) = 1 + \frac{2}{\pi} P \int_0^\infty \frac{\omega' \varepsilon_2(\omega')}{\omega'^2 - \omega^2} d\omega' \quad (10)$$

The real and the imaginary parts allow to calculate the absorption coefficient given as follows

$$\alpha(\omega) = \sqrt{2} \omega \left[\sqrt{\varepsilon_1^2(\omega) + \varepsilon_2^2(\omega)} - \varepsilon_1(\omega) \right]^{1/2} \quad (11)$$

The absorption coefficient $\alpha(\omega)$ is a fundamental parameter in evaluating the optical performance of materials, particularly for solar cell (SC) applications. It measures the efficiency with which a material absorbs incident light energy, reflecting its ability to convert light into electrical energy. Figure 3 shows the variation of the absorption coefficient as a function of photon energy. For candidate solar cell materials, typical absorption coefficient values are between 10^4 and 10^6 cm^{-1} . In the infrared region, the absorbance reaches approximately $2.5 \times 10^4 \text{ cm}^{-1}$, reflecting moderate interaction with low-energy photons. In the visible region between (1.65 and 3.26 eV), a more pronounced absorption is observed, with a peak reaching $6.7 \times 10^4 \text{ cm}^{-1}$, which represents a promising threshold for efficient absorption of sunlight. Progressing towards the ultraviolet region, a sharp increase is noted: the absorbance peaks at $2.5 \times 10^4 \text{ cm}^{-1}$ for a photon energy of approximately 9.03 eV, illustrating a highly absorbing behavior favorable to UV photodetectors and high-performance optoelectronic devices.

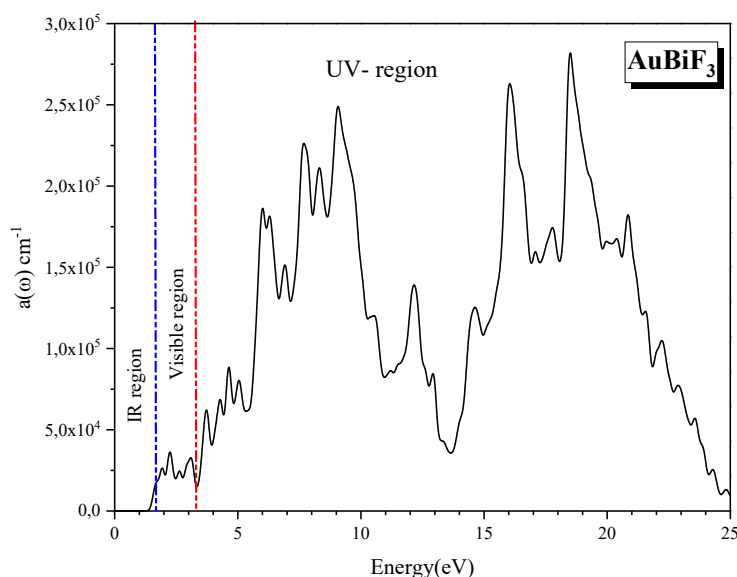


Figure 4. Calculated absorption coefficient using GGA-PBE for AuBiF₃ perovskite.

7. Conclusion

The rapid advancement of photovoltaic technologies, particularly tandem solar cells, requires materials with both high absorption capacity and reliable mechanical stability. The AuBiF₃ perovskite was studied using density functional theory (DFT) to characterize its structural, electronic, and optical characteristics. Electronic analysis indicates a direct band gap of 1.51 eV using HSE06 functional, which coincides with the ideal energy window for the lower layers in tandem multijunction architectures. The optical properties, such as absorption coefficient, demonstrate good absorption in the infrared, visible and ultraviolet regions, suggesting strong photonic interaction in the visible, and near-infrared regions, which is essential for high efficiency. These properties position AuBiF₃ as a strong candidate for next-generation photovoltaic devices, particularly in high-performance tandem cells and multifunctional optoelectronic applications. These results provide a solid theoretical foundation for future experimental work and practical integration on an industrial scale.

References

- [1] P. Basumatary, P. Agarwal, A short review on progress in perovskite solar cells, Mater. Res. Bull., 149 (2022) 111700.
- [2] M. Younas, T.A. Kandiel, A. Rinaldi, Q. Peng, A.A. Al-Saadi, Ambient-environment processed perovskite solar cells: a review, Materials Today Physics, 21 (2021) 100557.
- [3] J. Liao, X. Zhang, S. Guo, S. Zhang, X. Hu, Y. Chen, Fabrication and challenges for high-efficiency and up-scale perovskite solar modules, J. Mater. Chem., 12 (44) (2024) 17720-17741.
- [4] Q.A. Akkerman, L. Manna, What defines a halide perovskite?, ACS energy letters, 5 (2) (2020) 604-610.
- [5] P. Roy, A. Ghosh, F. Barclay, A. Khare, E. Cuce, Perovskite solar cells: A review of the recent advances, Coatings, 12 (8) (2022) 1089.

- [6] A.W. Faridi, M. Imran, G.H. Tariq, S. Ullah, S.F. Noor, S. Ansar, F. Sher, Synthesis and characterization of high-efficiency halide perovskite nanomaterials for light-absorbing applications, *Industrial & Engineering Chemistry Research*, 62 (11) (2022) 4494-4502.
- [7] F. Cao, L. Bian, L. Li, Perovskite solar cells with high-efficiency exceeding 25%: A review, *Energy Mater. Devices*, 2 (1) (2024) 9370018.
- [8] R.H. Friend, D. Di, S. Lilliu, B. Zhao, Perovskite LEDs, *Scientific Video Protocols*, 1 (1) (2019) 1-5.
- [9] R. Dong, Y. Fang, J. Chae, J. Dai, Z. Xiao, Q. Dong, Y. Yuan, A. Centrone, X.C. Zeng, J. Huang, Photodetectors: High-Gain and Low-Driving-Voltage Photodetectors Based on Organolead Triiodide Perovskites (*Adv. Mater.* 11/2015), *Adv. Mater.*, 27 (11) (2015) 1967-1967.
- [10] X. Lu, X. Fan, H. Zhang, Q. Xu, M. Ijaz, Review on preparation of perovskite solar cells by pulsed laser deposition, *Inorganics*, 12 (5) (2024) 128.
- [11] Y. Li, D. Maldonado-Lopez, V. Ríos Vargas, J. Zhang, K. Yang, Stability diagrams, defect tolerance, and absorption coefficients of hybrid halide semiconductors: High-throughput first-principles characterization, *J. Chem. Phys.*, 152 (8) (2020).
- [12] A. Kumar, S. Singh, M.K. Mohammed, A.E. Shalan, Effect of 2D perovskite layer and multivalent defect on the performance of 3D/2D bilayered perovskite solar cells through computational simulation studies, *Solar Energy*, 223 (2021) 193-201.
- [13] G. Tong, L.K. Ono, Y. Qi, Recent progress of all-bromide inorganic perovskite solar cells, *Energy Technology*, 8 (4) (2020) 1900961.
- [14] J. Tao, C. Zhao, Z. Wang, Y. Chen, L. Zang, G. Yang, Y. Bai, J. Chu, Suppressing non-radiative recombination for efficient and stable perovskite solar cells, *Energy Environ. Sci.*, 18 (2) (2025) 509-544.
- [15] M.S. Reza, M.S. Reza, A. Ghosh, M.F. Rahman, J.R. Rajabathar, F. Ahmed, M. Sajid, M.F.I. Buian, J. Bhandari, M.A. Islam, New highly efficient perovskite solar cell with power conversion efficiency of 31% based on Ca_3NI_3 and an effective charge transport layer, *Optics Communications*, 561 (2024) 130511.
- [16] D.H. Kim, C.P. Muzzillo, J. Tong, A.F. Palmstrom, B.W. Larson, C. Choi, S.P. Harvey, S. Glynn, J.B. Whitaker, F. Zhang, Bimolecular additives improve wide-band-gap perovskites for efficient tandem solar cells with CIGS, *Joule*, 3 (7) (2019) 1734-1745.
- [17] M.N.A. Dipon, M.A. Sahriar, S. Sarker, M.T. Islam, A. Rauf, M.R.H. Abed, A.R. Nirjhar, S.J. Tan-Ema, K.M. Shorowordi, S. Ahmed, A comprehensive study of mechanically stacked tandem photovoltaic devices: materials selection and efficiency analysis using SCAPS, *Energy Convers. Manage.*, 300 (2024) 117904.
- [18] V. Milman, K. Refson, S. Clark, C. Pickard, J. Yates, S.-P. Gao, P. Hasnip, M. Probert, A. Perlov, M. Segall, Electron and vibrational spectroscopies using DFT, plane waves and pseudopotentials: CASTEP implementation, *Journal of Molecular Structure: THEOCHEM*, 954 (1-3) (2010) 22-35.
- [19] H. Peng, J.P. Perdew, Rehabilitation of the Perdew-Burke-Ernzerhof generalized gradient approximation for layered materials, *Phys. Rev. B.*, 95 (8) (2017) 081105.
- [20] J. Heyd, J.E. Peralta, G.E. Scuseria, R.L. Martin, Energy band gaps and lattice parameters evaluated with the Heyd-Scuseria-Ernzerhof screened hybrid functional, *J. Chem. Phys.*, 123 (17) (2005).
- [21] M. Fuchs, M. Bockstedte, E. Pehlke, M. Scheffler, Pseudopotential study of binding properties of solids within generalized gradient approximations: The role of core-valence exchange correlation, *Phys. Rev. B.*, 57 (4) (1998) 2134.
- [22] A. Seidl, A. Görling, P. Vogl, J.A. Majewski, M. Levy, Generalized Kohn-Sham schemes and the band-gap problem, *Phys. Rev. B.*, 53 (7) (1996) 3764.

- [23] Y. Wang, P. Wisesa, A. Balasubramanian, S. Dwaraknath, T. Mueller, Rapid generation of optimal generalized Monkhorst-Pack grids, *Comput. Mater. Sci.*, 187 (2021) 110100.
- [24] Y. Nassah, A. Benmakhlouf, L. Hadjeris, T. Helaimia, R. Khenata, A. Bouhemadou, S. Bin Omran, R. Sharma, S. Goumri Said, V. Srivastava, Electronic band structure, mechanical and optical characteristics of new lead-free halide perovskites for solar cell applications based on DFT computation, *Bull. Mater. Sci.*, 46 (2) (2023) 55.
- [25] C. Truesdell, Murnaghan's Finite Deformation of an Elastic Solid (1952), in: *An Idiot's Fugitive Essays on Science: Methods, Criticism, Training, Circumstances*, Springer, 1984, pp. 148-150.
- [26] J. Wang, J. Li, S. Yip, D. Wolf, S. Phillpot, Unifying two criteria of Born: Elastic instability and melting of homogeneous crystals, *Physica A: Statistical Mechanics and its Applications*, 240 (1-2) (1997) 396-403.
- [27] O. Senkov, D. Miracle, Generalization of intrinsic ductile-to-brittle criteria by Pugh and Pettifor for materials with a cubic crystal structure, *Scientific reports*, 11 (1) (2021) 4531.
- [28] J.N. Hilfiker, T. Tiwald, Dielectric function modeling, in: *Spectroscopic Ellipsometry for Photovoltaics: Volume 1: Fundamental Principles and Solar Cell Characterization*, Springer, 2019, pp. 115-153.
- [29] H. Kuzmany, H. Kuzmany, The dielectric function, *Solid-State Spectroscopy: An Introduction*, (1998) 101-120.
- [30] M. Orazem, J. Esteban, O. Moghissi, Practical applications of the Kramers-Kronig relations, *Corrosion*, 47 (4) (1991) 248-259.